

PFC/JA-91-28

**Numerical Studies of the Spectral
Evolution of a Narrow-Bandwidth
FEL Oscillator***

Yang, T.-Y.B.; Temkin, R.J.; Kodama, S.;
Chen, S.C.; Danly, B.G.

Plasma Fusion Center
Massachusetts Institute of Technology
Cambridge, MA 02139

September 1991

[Faint, illegible handwritten signature]

Submitted to Nuclear Instruments & Methods and Physics Research A.

*This work was performed for MIT Lincoln Laboratory under Air Force Contract F19628-90-C-0002.

Numerical Studies of the Spectral Evolution of a Narrow-Bandwidth FEL Oscillator*

T.-Y. B. Yang, R. J. Temkin, S. Kodama, S. C. Chen and B. G. Danly

Plasma Fusion Center
Massachusetts Institute of Technology
Cambridge, Massachusetts 02139

October 1, 1991

ABSTRACT

The design study of an FEL oscillator with a bandwidth of $\Delta\omega/\omega_0 < 10^{-5}$ has been carried out. In this conceptual design, a grating rhomb is used to suppress the sideband instability. The spectral evolution of the FEL has been simulated using a one-dimensional, time-dependent FEL code. The system parameters for the simulations are: electron beam energy 120MeV, current $I = 50A$, electron micropulse length $\delta t_p = 330ps$, optical wavelength $\lambda_s = 0.5\mu m$, and wiggler period $\lambda_w = 2cm$. The detailed dependence of the spectral bandwidth on the frequency chirp introduced by the grating rhomb was investigated. A signal with FWHM bandwidth $\Delta\omega/\omega_0 = 4. \times 10^{-6}$ was obtained in a simulation using a large chirp parameter $\tau_s/\delta t_p = 80$, where τ_s is the time lag of the sideband (with $\Delta\omega/\omega_0 = -0.01$) behind the central frequency.

*This work was performed for MIT Lincoln Laboratory under Air Force Contract F19628-90-C-0002.

1 Introduction

There is growing experimental and theoretical evidence that free-electron lasers are effective sources of coherent radiation generation by intense relativistic electron beams. In the oscillator configuration, an FEL starts with small amplitude incoherent radiation in the resonator. Through the FEL interaction, the amplitude of the radiation grows and the bandwidth narrows. When the radiation amplitude is small and the system is in the linear regime, the bandwidth narrows significantly, because different Fourier components experience different gains in the resonator[1]. However, when the system is near saturation, nonlinear effects have a strong influence on the spectral evolution. One effect which may result in broadening the bandwidth of an FEL oscillator is the sideband instability[2-6].

Several sideband suppression techniques have been proposed theoretically and/or used in numerical simulations and experiments. It has been demonstrated, when the pulse length is not much longer than the slippage length, that the sidebands can be suppressed by adjusting the cavity length of the resonator[3]. However, a frequency selective component[5, 6] is usually required to suppress the sidebands when the pulse length is much longer than the slippage length. As has been demonstrated recently in numerical simulations[6], a negative frequency-chirp introduced by a grating rhomb not only suppresses the unstable sidebands, but also affects the pulse length and the phase profile of the optical beam, which in turn determines the bandwidth of the output signal.

In the present work, we investigated the possibility of designing a FEL oscillator of moderate time-average power, 1 to 10kW, capable of generating narrow bandwidth ($\Delta\omega/\omega_0 < 10^{-5}$) optical signals. Numerical simulations were carried out using a one-dimensional time-dependent FEL code developed at the M.I.T. Plasma Fusion Center. Detailed dependence of the bandwidth on the frequency chirp introduced by the grating rhomb was studied. Similar to what was observed in Ref.[6], it was found that the chirp parameter $\tau_s/\delta t_p$ is influential in determining the pulse shape, phase profile and the power spectrum of the optical signal. Here, δt_p designates the electron micropulse length, and τ_s is the time lag behind the central frequency of the most unstable sideband with $\Delta\omega/\omega_0 = -0.01$, after being passed through the grating rhomb. Utilizing a 330ps (micropulse length) square pulse electron beam incorporated with a large negative frequency chirp, a FWHM bandwidth of $\Delta\omega/\omega_0 = 4. \times 10^{-6}$ was achieved within the present simplified one-dimensional model.

2 Theoretical Model and Equations

For simplicity, we consider in this work only a circularly polarized magnetostatic wiggler. The equations for other types of wigglers are very similar to those employed in this paper and can be found, for example in ref. [7] for the linearly polarized magnetostatic wiggler and in ref. [8] for the electromagnetic wiggler.

The circularly polarized wiggler and the induced electromagnetic field of the same polarization are characterized by the transverse vector potential $\mathbf{A}_\perp = (A_x, A_y)$, which can be written as

$$A_x + iA_y = \frac{mc}{e}(a_x + ia_y) = -\frac{mc}{e}a_w e^{-ik_w z} + \frac{mc}{e}a_s e^{i(k_s z - \omega_s t + \phi_s)}, \quad (1)$$

where, in the present one-dimensional model, $a_w = a_w(z)$ and $k_w = 2\pi/\lambda_w$ are the wiggler field amplitude and wavenumber, while $a_s = a_s(z, t)$, $\phi_s = \phi_s(z, t)$, k_s and ω_s are the real amplitude, phase, wavenumber and frequency, respectively, of the transverse electromagnetic field. The complex amplitude $a_s e^{i\phi_s}$ is assumed to be a slowly varying function of both the longitudinal coordinate z and the time t (eikonal approximation), i.e.

$$|(\partial/\partial z) \ln a_s e^{i\phi_s}| \ll k_s, \quad |(\partial/\partial t) \ln a_s e^{i\phi_s}| \ll \omega_s. \quad (2)$$

In the one-dimensional approximation, all the electrons are assumed to be on ideal orbits with $\mathbf{p}_\perp = 0$. Moreover, the averaged motion of an electron in the combined wiggler and electromagnetic fields is determined by the following first-order equations[9]:

$$\frac{d\gamma}{dz} = -\frac{\omega_s}{\gamma c} a_w a_s \sin(\theta + \phi_s), \quad (3)$$

$$\frac{d\theta}{dz} = k_w - \frac{\omega_s}{c} \frac{1 + a_w^2 + a_s^2 - 2a_w a_s \cos(\theta + \phi_s)}{2\gamma^2}, \quad (4)$$

$$\frac{d(ct)}{dz} = 1 + \frac{1 + a_w^2 + a_s^2 - 2a_w a_s \cos(\theta + \phi_s)}{2\gamma^2}, \quad (5)$$

where γ is the relativistic mass factor of the electron, and the electron "phase" θ is defined by

$$\theta(z) = (k_w + k_s)z - \omega_s t(z). \quad (6)$$

In deriving Eqs. (3)-(5), it has been assumed that the electron beam is tenuous so that the longitudinal perturbations can be neglected (Compton-regime approximation with $\delta\phi = 0$)[9].

The evolution of the transverse electromagnetic field can be determined from the Maxwell equations. In the eikonal approximation, the slow nonlinear evolution of the complex amplitude $a_s \exp(i\phi_s)$ is described by[9]

$$2ik_s \left(\frac{\partial}{\partial z} + \frac{1}{v_g} \frac{\partial}{\partial t} \right) a_s e^{i\phi_s} = -\frac{eZ_0}{mc^2} \left\langle \frac{a_w e^{-i\theta}}{\gamma} \right\rangle, \quad (7)$$

where $Z_0 = \mu_0 c$ is the impedance of free space, and $v_g = c^2 k_s / \omega_s$ is the group velocity of the transverse electromagnetic wave. Furthermore, the angle brackets stand for the ensemble average over the electron distribution. In the numerical model used in the present analysis, the brackets denote a sum over the N_p particles, which carry a charge density $Q/N_p A_b$ each, defined as follows

$$\langle \dots \rangle = \frac{Q}{N_p A_b} \sum_{j=1}^{N_p} \delta[t - t_j(z)] (\dots). \quad (8)$$

Here, Q and A_b are, respectively, the total charge and the cross-section of the electron pulse injected into the wiggler.

To study the nonlinear time-dependent evolution of a free-electron laser, a computer code (TDS) which solves self-consistently Eqs. (3)-(5) and (7) has been developed. The numerical approach used in this code has been described in detail by Tran and Wurtele[9], and will not be repeated here.

Electron Beam Energy	120 MeV
γ	235.795
Electron Micropulse Length (Square Pulse)	330 ps
Electron Beam Current	50A
Electron Beam Radius	0.4 mm
Helical Wiggler	
Wiggler Period	2.0 cm
Wiggler Length (Untapered)	2.0 m
Wiggler Magnetic Field	1.0T
a_w	1.33
Optical Wavelength	0.5 μm
Optical Beam Radius	0.4 mm
Cavity Loss	24%
Rhomb Dispersion, $\tau_s/\delta t_p$	> 1.0

Table 1: Optical FEL simulation parameters

3 Numerical Simulations

A. System Parameters

The 1-D time-dependent FEL code (TDS) has been used to simulate the nonlinear evolution of a long-pulse (electron beam micropulse length=330ps), narrow-bandwidth (designed optical beam bandwidth $\Delta\omega/\omega < 10^{-5}$) optical FEL oscillator. Table 1 shows the system parameters used in the simulations. In the present 1-D model, the emittance of the electron beam has been ignored. Moreover, the current and beam radius of the electron beam are assigned only for the purpose of calculating the more relevant parameter, current density (current / area). Similarly, the power and radius of the optical beam are used only in determining the power density (power / area) of the beam. It has also been assumed that the electron beam has no energy spread ($\Delta\gamma = 0$).

It was found in the present one-dimensional simulations using the system parameters in Table 1 that the oscillator had a power level of 72MW in the cavity when it reached a steady state. With the 24% cavity loss, this implies a 31.6% single-pass gain and a 0.3% efficiency. Furthermore, the power and the efficiency can be significantly increased using a properly tapered wiggler, which was not included in the present simulations. A lower power and efficiency, however, should be expected if the energy spread and the emittance of the electron beam were taken into account.

B. Grating Rhomb

In the present numerical simulations, the effect of the grating rhomb is modelled by a phase shift which is a function of frequency[6, 10]

$$\phi(\omega) = \phi_0 + \tau_0(\omega - \omega_0) - \frac{(\omega - \omega_0)^2}{2\mu}, \quad (9)$$

where ω_0 is the central frequency corresponding to the wavelength $\lambda_s = 0.5\mu\text{m}$. Here, τ_0 is chosen such that the round trip time of the fourier component with frequency ω_0 is exactly equal to the separation between adjacent electron micropulses, and μ is determined by the condition that after one transit through the grating rhomb the most unstable sideband should not overlap with the electron beam. A simulation without a grating rhomb indicated that a strong sideband with frequency shift of $\Delta\omega_s/\omega_0 \simeq -0.01$ was developed after the system had saturated. Therefore, the condition for choosing μ is $\tau_s/\delta t_p > 1$. Here, we have adopted the notation used in [6], where δt_p designates the electron micropulse length ($\delta t_p = 330\text{ps}$ in this case), and τ_s is the time lag of the most unstable sideband behind the central frequency, i.e., $\tau_s = -\Delta\omega_s/\mu = 0.01\omega_0/\mu$.

C. Boundary Conditions and Initial Conditions

In solving Eqs. (3)-(5) and (7), initial conditions must be provided at $z = 0$. In addition, boundary conditions in the t coordinate need to be specified for the complex amplitude $a_s \exp(i\phi_s)$. In the present work, the simulations are carried out within a 3.333ns-long temporal window, and periodic boundary conditions are assumed for $a_s \exp(i\phi_s)$. This gives a resolution of $\delta\omega/\omega_0 = 5.0 \times 10^{-7}$ in the frequency domain. The t coordinate is further discretized into time bins. The separation between adjacent time bins is $4.1667 \times 10^{-14}\text{sec}$ corresponding to 25 periods of oscillation for the optical wave with wavelength $\lambda_s = 0.5\mu\text{m}$. The discrete Fourier transform of $a_s \exp(i\phi_s)$ is then periodic in the ω domain with period $\Delta\omega = 1.508 \times 10^{14}\text{rad/sec}$ (or $\Delta\omega/\omega_0 = 0.04$).

To simulate an oscillator starting from noise, the complex amplitude $a_s \exp(i\phi_s)$, at the beginning ($z = 0$) of the first pass, is loaded such that its Fourier transform has a constant amplitude (independent of ω) and a phase which is a random distribution in ω . The amplitude is chosen such that the total radiation energy within the 3.333ns-long temporal window is $3.333\mu\text{J}$ (or 1kW average power) for an optical beam with a radius of 0.4mm. At the end of each pass, the complex amplitude $a_s \exp(i\phi_s)$ is passed through a filter which takes into account the cavity loss and the phase shift

due to the grating rhomb. The output from the filter will then be used as the initial conditions for the next pass. At the beginning of each pass ($z = 0$), the electron beam is loaded as a 330ps-long flat-top square pulse located at the center of the 3.333ns-long temporal window. The electrons are modelled by macroparticles with equal energies and charges. For each time bin within the square pulse, there are 11 macroparticles with their phases uniformly distributed in the interval between $-\pi$ and π .

For large chirp parameters $\tau_s/\delta t_p$, extra caution needs to be taken due to the fact that the periodic boundary condition applied to the 330ps temporal window can cause undesirable overlap of the electron pulse with some strongly unstable sidebands. When the radiation reaches a large power and the sidebands start to grow, an extra filter is introduced at the end of the cavity to filter out those sidebands which may undesirably overlap with the electron pulse. It should be noted that such a filter is introduced for solely mathematical reason. No filter is required in the real physical system, for the undesirable overlap of the electron beam and the sidebands does not really occur there.

D. Simulation Results

Numerical simulations of an optical FEL oscillator with system parameters given in Table 1 have been carried out for different choices of the chirp parameter $\tau_s/\delta t_p = 1.1423 \times 10^{23}/\mu$, where μ is in the unit of sec^{-2} . For each choice of the chirp parameter $\tau_s/\delta t_p$, the simulation was carried out for more passes than what are required to reach a steady state, except for the case with $\tau_s/\delta t_p = 1$, in which the system did not reach a steady state after 800 passes. It was found in the simulations that the larger the chirp parameter we chose, the fewer passes are required to reach a steady state; to give a rough estimate, about 40 passes are required for $\tau_s/\delta t_p = 80$, 80 passes for $\tau_s/\delta t_p = 50$, 140 passes for $\tau_s/\delta t_p = 30$, 180 passes for $\tau_s/\delta t_p = 10$, and more than 800 passes are required for $\tau_s/\delta t_p = 1$. This trend can easily explained by the fact that the grating rhomb introduces communication between different time bins, and the larger is the frequency chirp, the stronger is the communication.

Shown in Figs. 1 – 5, are the amplitude $|a_s|$, phase ϕ_s (as functions of time t) and the power spectrum of the optical beam at the end of the simulation for different choices of chirp parameter $\tau_s/\delta t_p$. At the steady state, assuming an optical beam with a radius of 0.4mm, the total radiation energy at the end of the wiggler region is around $2.4 \times 10^{-2}\text{J}$ (or 72MW average power within the 330ps pulse) for all choices of the chirp parameter. In Figs. 1 – 5, the amplitude and the phase are plotted

versus time. Moreover, the power spectra are plotted versus normalized frequency shift $\Delta\omega/\omega_0 = (\omega - \omega_0)/\omega_0$, where ω_0 is the central frequency corresponding to the wavelength $\lambda_s = 0.5\mu\text{m}$. The 330ps intervals at the bottoms of panels (a) and (b) in Figs. 1 – 5 indicate where the square-pulse electron beam would be located.

For the simulation with the choice of the chirp parameter $\tau_s/\delta t_p = 1$, the profile of the radiation amplitude still resembles a square pulse at the end of 800th pass [Fig. 1(a)]. The phase profile in Fig. 1(b), however, indicates that the front part (at smaller t) and the rear part (at larger t) of the radiation pulse experience different frequency shifts ($-d\phi_s/dt$). Consequently, the power spectrum in Fig. 1(c) has two peaks with separation equal to the frequency difference between the rear and the front of the radiation pulse.

Observing in Fig. 1(b) that the rear part of the radiation pulse has a larger frequency than the front part, i.e. the radiation pulse has a positive frequency chirp, we expected that an increase in the negative frequency chirp introduced by the grating rhomb [decrease μ in Eq. (9)] may reduce the frequency shift within the radiation pulse and narrow the power spectrum. Simulations carried out for different choices of the chirp parameter showed such a trend (see Figs. 1 – 5). To summarize the results showed in Figs. 1 – 5, an increase in the chirp parameter $\tau_s/\delta t_p$ has the following effects: (a) the number of passes required to reach a steady state decreases, (b) the radiation pulse shape has less resemblance to a square pulse, (c) the frequency chirp within the pulse decreases, and (d) the bandwidth of the power spectrum narrows. For the largest chirp parameter used ($\tau_s/\delta t_p = 80$), only 40 passes are required to reach a steady state, and the FWHM bandwidth of the radiation pulse is around $\Delta\omega/\omega_0 = 4 \times 10^{-6}$. Moreover, 70% of the radiation power lies within the FWHM bandwidth.

4 Conclusions

Simulations of a long-micropulse optical ($\lambda_s = 0.5\mu\text{m}$) FEL oscillator have been carried out using a one-dimensional time-dependent FEL code (TDS). The model of a grating rhomb has been implemented in the code in order to suppress the unstable sidebands. By varying the chirp parameter $\tau_s/\delta t_p$ in the simulations, we investigated the effects of the grating rhomb on the spectral evolution of the FEL oscillator. It was found that larger chirp parameters are favorable in achieving narrow bandwidths. For the system parameters in Table 1, a narrow bandwidth of $\Delta\omega/\omega_0 = 4 \times 10^{-6}$ was

obtained in a simulation with a large chirp parameter $\tau_s/\delta t_p = 80$. Finally, it should be noted that some realistic effects such as the emittance and energy spread of the electron beam, and the transverse variation of the radiation field were neglected in this work. A study of the spectral evolution which takes into account these realistic effects will be the subject of future investigation.

References

- [1] W. B. Colson, "Classical Free Electron Laser Theory", chapter 3 in *Free Electron Laser Handbook*, edited by W. B. Colson, C. Pellegrini and A. Renieri (North-Holland, Amsterdam, 1989).
- [2] N. M. Kroll, P. L. Morton and M. N. Rosenbluth, *IEEE J. Quantum Electron.* **QE-17**, 1436 (1981).
- [3] R. W. Warren, B. E. Newnam and J. C. Goldstein, *IEEE J. Quantum Electron.* **QE-21**, 882 (1985).
- [4] R. C. Davidson, *Phys. Fluids* **29**, 2689 (1986).
- [5] D. C. Quimby, J. M. Slater and J. P. Wilcoxon, *IEEE J. Quantum Electron.* **QE-21**, 979 (1985).
- [6] R. L. Tokar, B. D. McVey and J. C. Goldstein, *IEEE J. Quantum Electron.* **QE-24**, 856 (1988).
- [7] W. B. Colson, *IEEE J. Quantum Electron.* **QE-17**, 1417 (1981).
- [8] T. M. Tran, B. G. Danly and J. S. Wurtele, *IEEE J. Quantum Electron.* **QE-23**, 1578 (1987).
- [9] T. M. Tran, J. S. Wurtele, *Physics Reports*, Vol. 195, No. 1, 1 (1990).
- [10] E. B. Treacy, *IEEE J. Quantum Electron.* **QE-5**, 454 (1969).

Figure Captions

- Fig. 1** Results at the end of 800th pass for a simulation with the choice of the chirp parameter $\tau_s/\delta_p = 1$. Shown are (a) the amplitude $|a_s|$ and (b) the phase ϕ_s of the radiation field versus t , and (c) the power spectrum as a function of the normalized frequency shift $\Delta\omega/\omega_0 \equiv (\omega - \omega_0)/\omega_0$.
- Fig. 2** Results at the end of 250th pass for a simulation with the choice of the chirp parameter $\tau_s/\delta_p = 10$. Shown are (a) the amplitude $|a_s|$ and (b) the phase ϕ_s of the radiation field versus t , and (c) the power spectrum as a function of the normalized frequency shift $\Delta\omega/\omega_0 \equiv (\omega - \omega_0)/\omega_0$.
- Fig. 3** Results at the end of 200th pass for a simulation with the choice of the chirp parameter $\tau_s/\delta_p = 30$. Shown are (a) the amplitude $|a_s|$ and (b) the phase ϕ_s of the radiation field versus t , and (c) the power spectrum as a function of the normalized frequency shift $\Delta\omega/\omega_0 \equiv (\omega - \omega_0)/\omega_0$.
- Fig. 4** Results at the end of 150th pass for a simulation with the choice of the chirp parameter $\tau_s/\delta_p = 50$. Shown are (a) the amplitude $|a_s|$ and (b) the phase ϕ_s of the radiation field versus t , and (c) the power spectrum as a function of the normalized frequency shift $\Delta\omega/\omega_0 \equiv (\omega - \omega_0)/\omega_0$.
- Fig. 5** Results at the end of 50th pass for a simulation with the choice of the chirp parameter $\tau_s/\delta_p = 80$. Shown are (a) the amplitude $|a_s|$ and (b) the phase ϕ_s of the radiation field versus t , and (c) the power spectrum as a function of the normalized frequency shift $\Delta\omega/\omega_0 \equiv (\omega - \omega_0)/\omega_0$.

$\tau_s/\delta t_p=1$, 800th pass

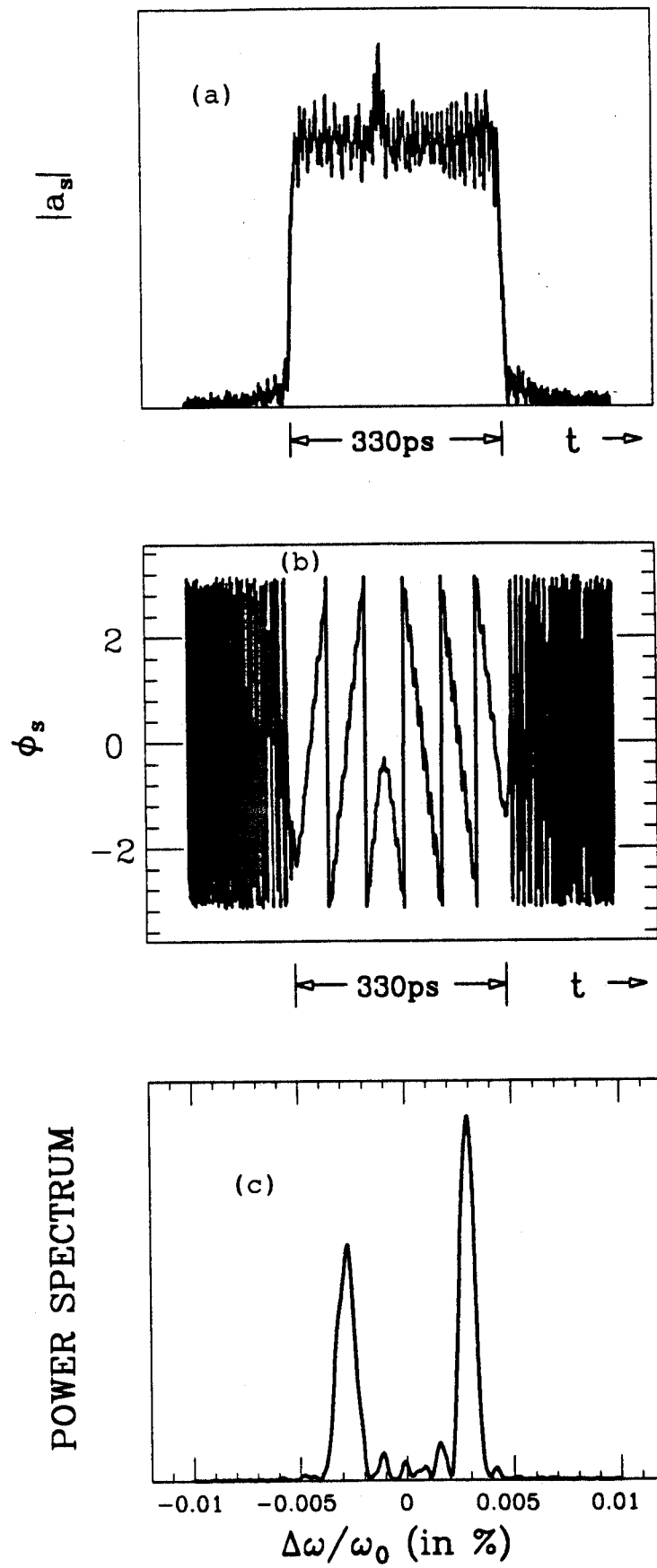


Fig. 1

$\tau_s/\delta t_p=10$, 250th pass

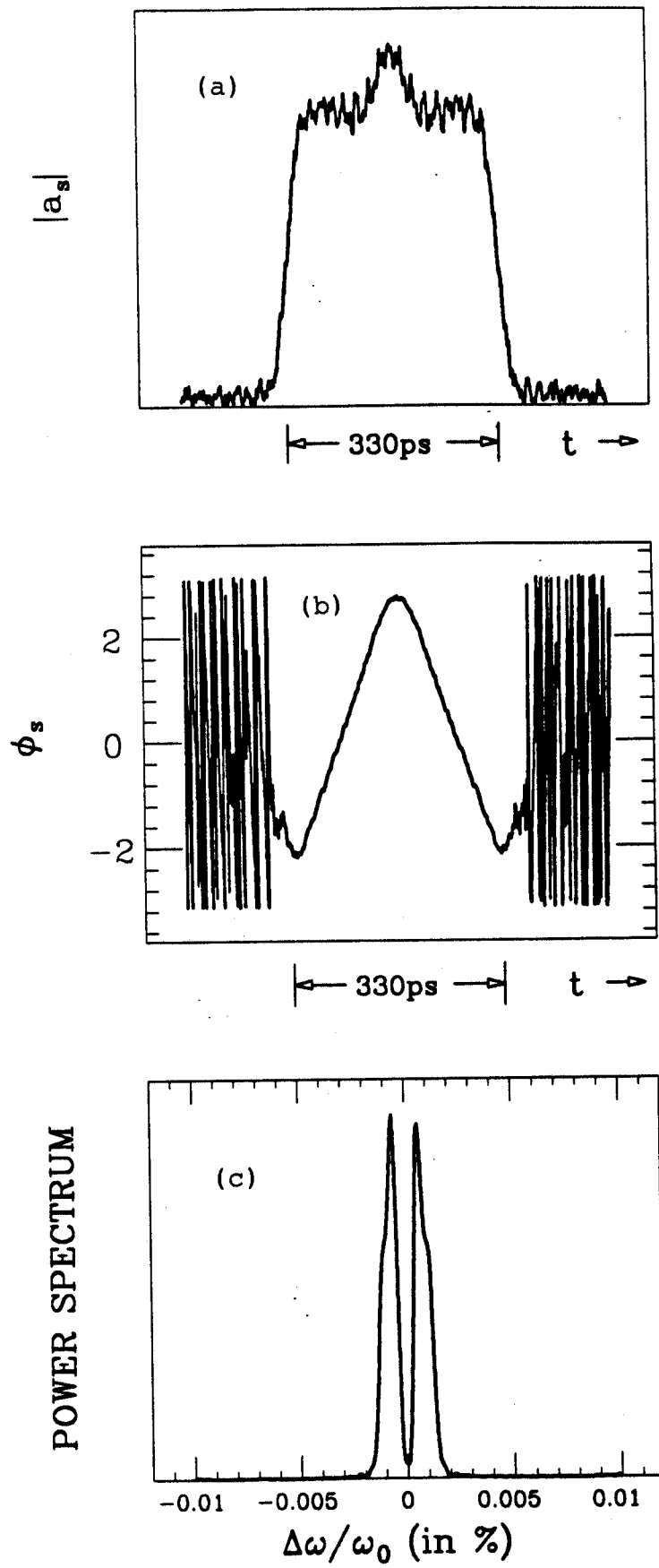


Fig. 2

$\tau_s/\delta t_p=30$, 200th pass

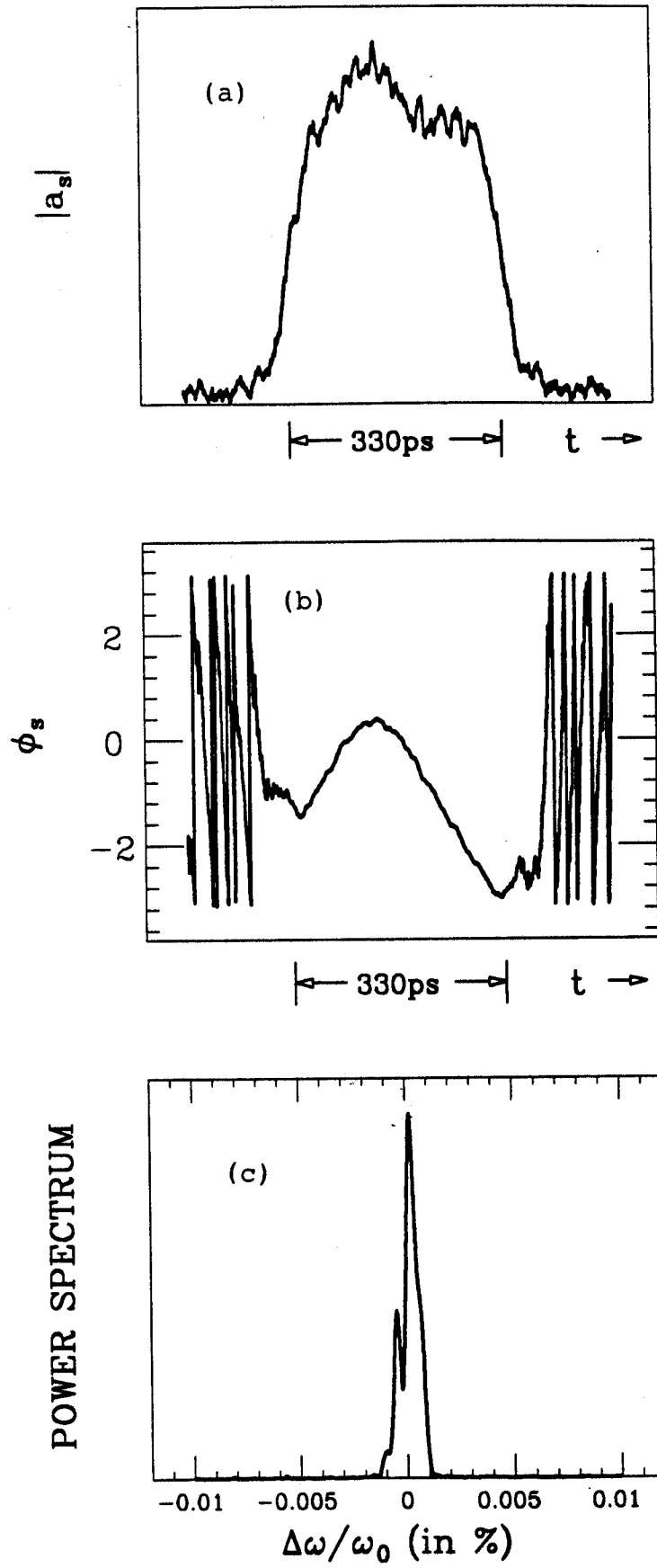


Fig. 3

$\tau_s/\delta t_p=50$, 150th pass

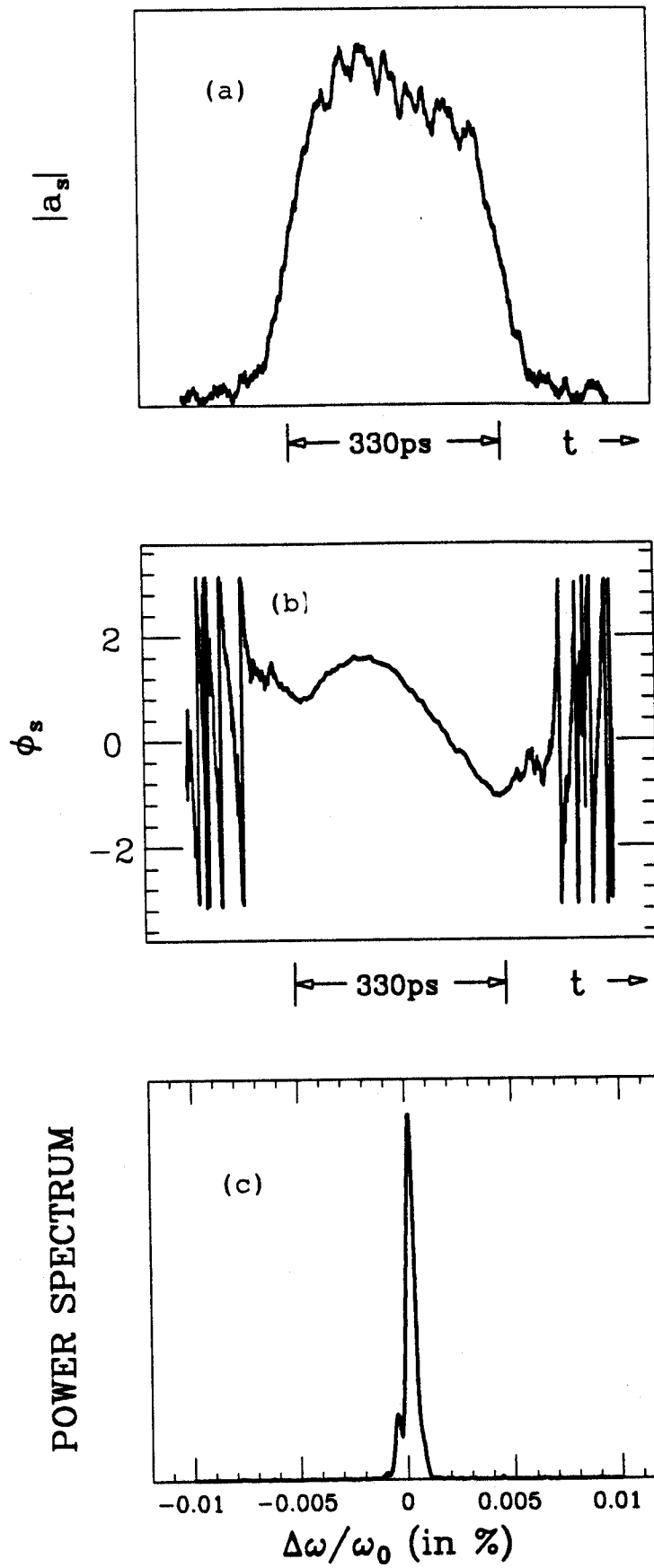


Fig. 4

$\tau_s/\delta t_p=80$, 50th pass

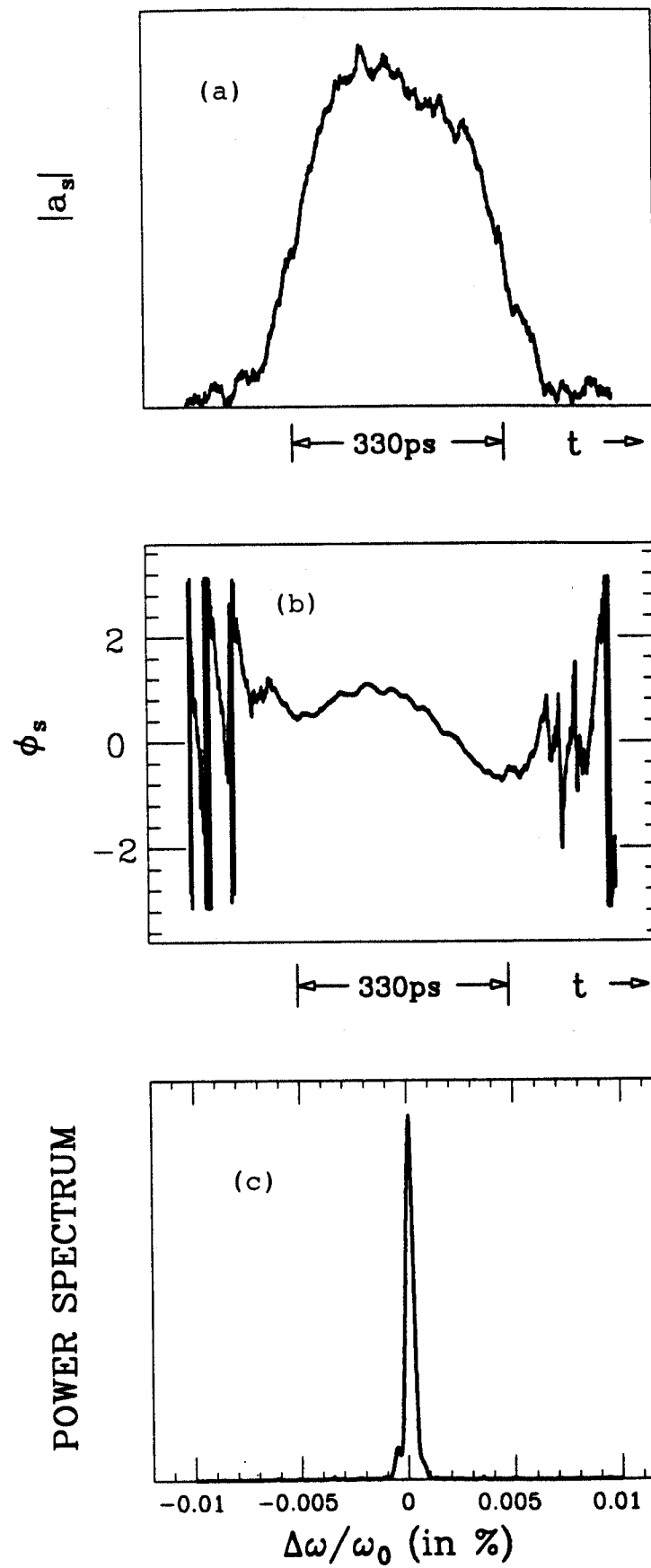


Fig. 5